

## The effect of random matter density perturbations on the MSW solution to the solar neutrino problem

H. Nunokawa <sup>\*</sup>, A. Rossi <sup>†</sup>, V. B. Semikoz <sup>‡</sup> and J. W. F. Valle <sup>§</sup>

*Instituto de Física Corpuscular - C.S.I.C.  
Departament de Física Teòrica, Universitat de València  
46100 Burjassot, València, SPAIN*

### Abstract

We consider the implications of solar matter density random noise upon resonant neutrino conversion. The evolution equation describing MSW-like conversion is derived in the framework of the Schrödinger approach. We study quantitatively their effect upon both large and small mixing angle MSW solutions to the solar neutrino problem. This is carried out both for the active-active  $\nu_e \rightarrow \nu_{\mu,\tau}$  as well as active-sterile  $\nu_e \rightarrow \nu_s$  conversion channels. We find that the small mixing MSW solution is much more stable (especially in  $\Delta m^2$ ) than the large mixing solution. The possible existence of solar matter density noise at the few percent level could be tested at future solar neutrino experiments, especially Borexino.

---

<sup>\*</sup> E-mail: nunokawa@flamenco.ific.uv.es, nunokawa@titan.ific.uv.es

<sup>†</sup> E-mail: rossi@evalvx.ific.uv.es, rossi@ferrara.infn.it

<sup>‡</sup> E-mail: semikoz@evalvx.ific.uv.es;

On leave from the *Institute of the Terrestrial Magnetism, the Ionosphere and Radio Wave Propagation of the Russian Academy of Sciences, IZMIRAN, Troitsk, Moscow region, 142092, Russia.*

<sup>§</sup> E-mail: valle@flamenco.ific.uv.es

# 1. Introduction

The long-standing deficit of solar neutrinos (the Solar Neutrino Problem (SNP)) has now been observed by all four operating experiments [1,2,3,4,5]. The main essence of the SNP is the strong deficit of the beryllium neutrinos [6]. On the other hand, the high energy boron neutrinos are moderately suppressed, while the low energy ones are almost undepleted. This strongly suggests that any astrophysical solution fails [6,7] in reconciling the experimental data with the Standard Solar Model (SSM) predictions [8,9,10].

It is possible to ascribe the solar neutrino deficit to the existence of two types of neutrino conversion mechanisms, both of which can deplete neutrinos of different energies differently, as required by the experimental data. The long wavelength vacuum oscillations provide a good fit to the most recent results for  $\Delta m^2 \simeq 10^{-10} \text{eV}^2$  and large neutrino mixing  $\sin^2 2\theta \simeq 1$  [11,12,13]. The other scenario is the resonant neutrino conversion due to interactions with constituents of the solar material (the Mikheyev-Smirnov-Wolfenstein (MSW) effect) [14]. This provides an extremely good data fit in the small mixing region with  $\Delta m^2 \simeq 10^{-5} \text{eV}^2$  and  $\sin^2 2\theta \simeq 10^{-3} \div 10^{-2}$  [15,16,13]. Both of these solutions have been studied against possible changes of the SSM input parameters [16,12]. For example, the study of the MSW effect has revealed its stability, especially in the  $\Delta m^2$  parameter.

In this paper we investigate the stability of the MSW solution with respect to the possible presence of random perturbations in the solar matter density, so far not included in the standard MSW picture.

In Ref. [17] the effect of periodic matter density perturbations added to an average density  $\rho_0$ , i.e.

$$\rho(r) = \rho_0[1 + h \sin(\gamma r)] \quad (1.1)$$

upon resonant neutrino conversion was investigated. The major effects show up when the fixed frequency ( $\gamma$ ) of the perturbation is close to the neutrino oscillation eigen-frequency, and for rather large amplitude values ( $h \sim 0.1 - 0.2$ ), giving rise to the parametric effects [17]. Such effects can either enhance or suppress neutrino conversion in the Sun. There are also a number of papers which address similar effects by different approaches [18,19].

Direct observations of solar surface motions, resulting from the superposition of several modes, may indicate a rich spectrum of frequencies. This would suggest the need to consider the effect of random or "white" noise matter density perturbations  $\xi(r)$ , characterised by an *arbitrary* wave number  $k$ ,

$$\xi(r) = \int dk \xi(k) \sin kr, \quad (1.2)$$

rather than a periodic or regular perturbation. In such a case the spatial correlation function for a uniform medium

$$\langle \xi(r_1) \xi(r_2) \rangle = \langle \xi^2 \rangle_{r_1 - r_2}, \quad (1.3)$$

obeys  $\langle \xi(k) \xi(k') \rangle = \langle \xi^2 \rangle_k \delta(k + k')$  as the averaging rule for the Fourier components, where the wave number  $k$  is not fixed. The effect of solar density as well as solar magnetic field fluctuations upon neutrino spin-flavour conversions has also been considered in Ref. [19], using somewhat different methods.

In this paper, after some discussion (Sec. 2) about the nature of the matter density fluctuations, we derive the most general neutrino evolution equation in random matter, starting from the standard Schrödinger equation (Sec. 3). This discussion is closer to the particle physics intuition than that of Ref. [19]. Moreover, we consider both the active-active  $\nu_e \rightarrow \nu_{\mu,\tau}$  as well as the active-sterile  $\nu_e \rightarrow \nu_s$  neutrino conversion channels (here  $\nu_s$  is a neutrino state with no standard model interaction). The latter is motivated by the fact that the existence of a sterile neutrino seems to be the only way to simultaneously account for the solar and atmospheric neutrino deficits in the presence of neutrino dark matter [20].

After an analytical study of the neutrino conversion equations we have investigated the impact of matter density noise upon the MSW scenario in the context of the SNP (Sec. 4). Typically, we find that the presence of matter fluctuations weakens the MSW mechanism, thus reducing the resonant conversion probabilities [19]. We have carried out a fit of the latest solar neutrino data for different values of the noise level, minimising the  $\chi^2$  in the  $(\Delta m^2, \sin^2 2\theta)$  plane. As in the noiseless MSW case, we find that the small mixing MSW solution provides a better fit to the data than the large mixing one, both for the case of active, as well as sterile neutrino conversions. We present several plots with the results of our fits in which the effect of the noise is studied in the idealised approximation where all neutrinos are produced at the solar centre. We conclude that the most relevant parameter region corresponding to adiabatic conversion of  ${}^7\text{Be}$  neutrinos is relatively stable with respect to such density fluctuations, whereas there is a larger effect of the noise for the large mixing MSW solution. We show how the possible existence of solar matter density noise could be tested in the next generation of solar neutrino experiments, especially Borexino. Finally, we comment on how possible solar model uncertainties could affect our results.

## 2. Matter Density Noise in the Sun

Let us briefly discuss the expected size of fluctuations in the Sun and their correlation lengths. For the sake of discussion, we can approximate (except in the very inner core) the average solar matter density, as given by the Standard Solar Model (SSM) [8,9,10], by:

$$\rho(r) \simeq \rho_0 \exp\left(-\frac{r - r_0}{R_0}\right) \quad (2.1)$$

where  $R_0 \approx 0.1R_s$  ( $R_s$  is the solar radius),  $r_0 \simeq 0$ , and  $\rho_0 \approx 250\text{g/cm}^3$ . The SSM in itself cannot account for the existence of density perturbations, since it is based on hydrostatic evolution equations.

One may however speculate upon possible mechanisms that could induce such density inhomogeneities in the Sun. Unfortunately it is quite difficult to give reliable estimates of the density perturbations in deep layers of the Sun, since this would require the detection of  $g$ -modes, not yet possible [21]. Indeed, these modes can exist only in deep layers beneath the convective zone and thus they can reach the surface only after an exponential damping through the convective zone [9]. Note also that it is extremely difficult to identify the  $g$ -modes in helioseismology observations, due to their tendency

to be accumulated in the lower frequency part of the Fourier spectrum. We may, however, give a simple estimate of the level of density perturbations  $\delta\rho$  in the solar interior by combining the continuity equation up to the first order in  $\delta\rho$  and the velocity perturbation  $\delta\mathbf{v}$

$$\frac{\partial\delta\rho}{\partial t} + \nabla \cdot \delta\mathbf{v}\rho = 0, \quad (2.2)$$

with the  $p$ -mode observations of the IRIS network at Tenerife [9]. These show that in the lower frequency part of the Fourier spectrum, the  $p$ -mode spectrum resembles that of noise, namely  $\sim 1/f$ . For instance, using the measured power  $\delta P = 10^3 \text{ m}^2 \text{ s}^{-1}$  corresponding to the frequency  $f = 10^{-4} \text{ s}^{-1}$  (see Fig. 26 of Ref. [9]) we may estimate from Eq. (2.2) the perturbation level  $\xi$  defined as

$$\xi = \frac{\delta\rho}{\rho} \equiv \frac{\sqrt{\langle\delta\rho^2\rangle}}{\rho}. \quad (2.3)$$

We obtain

$$\xi^2 \simeq \frac{\delta v^2}{f^2 L_0^2} = \frac{\delta P(f)}{f L_0^2} \sim \frac{10^3 \text{ m}^2 \text{ s}^{-1}}{10^{-4} \text{ s}^{-1} \times (10^6 \text{ m})^2} \sim 10^{-5} \quad (2.4)$$

where we have taken as typical size of the spatial inhomogeneity the value  $L_0 \sim 10^3 \text{ km}$ , the so-called "granule"-size. Thus we see that values  $\xi \sim 0.3\%$  in the solar surface can not be excluded. In contrast, inside the solar core the estimate of the parameter  $L_0$  becomes very rough. In fact one expects that, due to buoyancy, the  $g$ -mode amplitudes beneath the convective zone can be larger than at the surface and, correspondingly, the inhomogeneity size  $L_0$  smaller than at the edge of the Sun (see Fig. 13 (a) of Ref. [9]). As a result, for a fixed perturbation amplitude  $\delta v^2 = \text{const}$  we can extrapolate the *continuous* power spectrum to low frequencies leading to a large density inhomogeneities since  $\xi \sim f^{-1} L_0^{-1}$ .

There is another way to estimate the level of density fluctuations using the density profile of Eq. (2.1). Indeed, in the hydro-dynamical approximation, density perturbations can be induced by corresponding temperature  $T$  fluctuations due to convection of matter between layers with different local temperatures. For example, if we express the macroscopic matter density  $\rho(r)$  through the Boltzmann distribution with the gravitational potential energy  $U = m_p g(r)(r - r_0)$ , where  $g(r) = GM(r)/r^2$ ,  $G$  being Newton's constant,  $m_p$  the nucleon mass and  $M(r)$  the mass contained in a sphere of radius  $r$ . The change  $T \rightarrow T + \delta T$  leads to

$$\rho(r; T + \delta T) = \rho_0 \exp\left[-\frac{m_p g(r - r_0)}{T + \delta T}\right] = \rho(r; T)[1 + \xi],$$

where  $\xi \equiv \xi(r; T; \delta T)$ . From this we have

$$\xi = \frac{\delta\rho}{\rho} = \frac{m_p g(r - r_0)}{T} \frac{\delta T}{T} = \frac{(r - r_0)}{R_0} \frac{\delta T}{T}, \quad (2.5)$$

where we have compared the relevant exponent with that in eq. (2.1). One can argue that  $\sqrt{\langle\delta T^2\rangle}/T \lesssim 0.05$  is not in conflict neither with the SSM nor with present helioseismology observations [9,22]. Thus from Eq. (2.5),

taking  $(r - r_0)/R_0 \sim 1$ , we obtain a correspondingly comparable level of density fluctuations. Thus in what follows we assume the existence of such few percent level matter density fluctuations, up to 8%<sup>1</sup>.

Now we generalise the above discussion to the case in which the perturbation  $\delta\rho$  is of random nature. Following ref. [19] we assume that the random field  $\delta\rho$  is a  $\delta$ -correlated Gaussian distribution. For small inhomogeneities, the autocorrelation function  $\langle\xi^2\rangle$  can be taken as

$$\langle\delta\rho(r_1)\delta\rho(r_2)\rangle = 2\rho^2\langle\xi^2\rangle L_0\delta(r_1 - r_2) \quad (2.6)$$

whose correlation length  $L_0$  obeys the following relation:

$$l_{free} \ll L_0 \ll \lambda_m \quad (2.7)$$

where  $l_{free} = (\sigma n_0)^{-1}$  is the mean free path of the electrons in the Sun. This lower bound is dictated by the hydro-dynamical approximation used later. For Coulomb interactions, the cross-section  $\sigma$  is determined by the classical radius of electron  $r_{0e} = e^2/m_e c^2 \sim 2 \times 10^{-13}\text{cm}$ , resulting in  $l_{free} \sim 10\text{cm}$  for a solar mean density  $n_0 \sim 10^{24}\text{cm}^{-3}$  and  $\sigma \sim 10^{-25}\text{cm}^2$ . On the other hand, the upper bound expresses the fact that the scale of fluctuations should be much smaller than the characteristic neutrino matter oscillation length,  $\lambda_m$ , as indeed the  $\delta$ -correlation distribution in Eq. (2.6) requires.

### 3. Neutrino Conversion in Noisy Matter

Let us consider a system of two neutrinos  $\nu_e$  and  $\nu_x$ . In the case of active-active neutrino conversion  $x = \mu$  or  $\tau$ , while for the case of active-sterile neutrino conversions  $\nu_x = \nu_s$ , with  $\nu_s$  being the sterile state.

Neutrino propagation in the solar medium is affected by the coherent neutrino scattering off matter constituents which can be described in terms of the matter potential  $V$ . In the rest frame of the unpolarised matter, the potential is given, in the Standard Model, by

$$V = \frac{\sqrt{2}G_F}{m_p}\rho Y \quad (3.1)$$

where  $G_F$  is the Fermi constant,  $\rho$  is the matter density and  $Y$  is a number which depends on the neutrino type and on the chemical content of the medium. More precisely,  $Y = Y_e - \frac{1}{2}Y_n$  for the  $\nu_e$  state,  $Y = -\frac{1}{2}Y_n$  for  $\nu_\mu$  and  $\nu_\tau$  and  $Y = 0$  for the  $\nu_s$  state, where  $Y_{e,n}$  denotes the electron and neutron number per nucleon. The matter potential modifies the energy dispersion relations for neutrino states, leading to the phenomenon of resonant conversion (the MSW effect [14]). Let us note that in this respect the potential  $V$ , i.e. the function  $\rho$ , previously described, represents an average macroscopic quantity.

---

<sup>1</sup>Note that for an ideal plasma, like that in the Sun, the equilibrium plasma fluctuations are negligible [23],  $\xi = \langle\delta n_e^2\rangle^{1/2}/n_e \sim (n_e r_D^3)^{-1} \ll 1$ , where  $n_e$  is the electron density,  $\delta n_e$  the corresponding fluctuation and  $r_D = (T/4\pi e^2 n_e)^{1/2}$  the Debye radius. Since the number of particles inside the Debye radius is very large,  $N_D = n_e r_D^3 \gg 1$ , with  $r_D \sim 10^{-7}\text{cm} \ll l_{free}$  these fluctuations are irrelevant for our present discussion.

Now we re-derive the evolution equation for the neutrino in the presence of matter density random perturbations, which we regard as superimposed over the main average matter density profile. It is clear from Eq. (2.6) that the random component of the potential can be written as  $V(t)\xi^2$ .

The evolution for the  $\nu_e - \nu_y$  ( $y = x$  or  $y = s$ ) system is governed by

$$i\frac{d}{dt}\begin{pmatrix} \nu_e \\ \nu_y \end{pmatrix} = \begin{pmatrix} H_e & H_{ey} \\ H_{ey} & H_y \end{pmatrix} \begin{pmatrix} \nu_e \\ \nu_y \end{pmatrix}, \quad (3.2)$$

where the entries of the Hamiltonian matrix are given by <sup>3</sup>

$$\begin{aligned} H_e &= 2[A_{ey}(t) + \tilde{A}_{ey}(t)], & H_y &= 0, \\ A_{ey}(t) &= \frac{1}{2}[V_{ey}(t) - \frac{\Delta m^2}{2E} \cos 2\theta], & \tilde{A}_{ey}(t) &= \frac{1}{2}V_{ey}(t)\xi \end{aligned} \quad (3.3)$$

Here  $\theta$  is the neutrino mixing angle in vacuum,  $\Delta m^2$  is the neutrino squared mass difference, and the matter potential for the active-active neutrino conversion ( $y = x$ ) reads

$$V_{ex}(t) = \frac{\sqrt{2}G_F}{m_p}\rho(t)(1 - Y_n) \quad (3.4)$$

or alternatively in case of  $\nu_s$

$$V_{es}(t) = \frac{\sqrt{2}G_F}{m_p}\rho(t)(1 - \frac{3}{2}Y_n) \quad (3.5)$$

(the neutral matter relation  $Y_e = 1 - Y_n$  has been used).

The above system can be rewritten in terms of the following equations:

$$\begin{aligned} \dot{P}(t) &= 2H_{ey}I(t) \\ \dot{R}(t) &= -H_e(t)I(t) \\ \dot{I}(t) &= H_e(t)R(t) - H_{ey}(2P(t) - 1) \end{aligned} \quad (3.6)$$

where  $P = |\nu_e|^2$  is the  $\nu_e$  survival probability,  $R \equiv \text{Re}(\nu_y^*\nu_e)$  and  $I \equiv \text{Im}(\nu_y^*\nu_e)$ . The corresponding initial conditions are:

$$P(t_0) = 1, \quad I(t_0) = 0, \quad R(t_0) = 0. \quad (3.7)$$

Defining

$$\begin{aligned} R(t) \pm iI(t) &= e^{\pm i\int_{t_0}^t H_e(t_1)dt_1} Z_{\pm}(t) \\ Z_{\pm}(t) &= \mp i \int_{t_0}^t H_{ey}(2P(t_1) - 1) e^{\mp i\int_{t_0}^{t_1} H_e(t_2)dt_2} dt_1, \end{aligned} \quad (3.8)$$

we can express the auxiliary functions  $R(t)$  and  $I(t)$  as:

$$R(t) = \int_{t_0}^t H_{ey}(2P(t_1) - 1) \sin\left(\int_{t_1}^t H_e(t_2)dt_2\right) dt_1 \quad (3.9)$$

$$I(t) = -\int_{t_0}^t H_{ey}(2P(t_1) - 1) \cos\left(\int_{t_1}^t H_e(t_2)dt_2\right) dt_1. \quad (3.10)$$

---

<sup>2</sup>The radial dependence of the solar matter density is understood as a time dependence since neutrinos are relativistic.

<sup>3</sup>In the Hamiltonian matrix, a term proportional to the identity has been removed.

After substituting the Eqs. (3.9) and (3.10) in the r.h.s of (3.6), we can average over the random density distribution, taking into account that for the random component we have:

$$\langle \tilde{A}_{ey}^{2n+1} \rangle = 0, \quad \langle \tilde{A}_{ey}(t)\tilde{A}_{ey}(t_1) \rangle = 2\kappa\delta(t-t_1), \quad (3.11)$$

where the quantity  $\kappa$  is defined as

$$\kappa(t) = \langle \tilde{A}_{ey}^2(t) \rangle L_0 = \frac{1}{4} V_{ey}^2(t) \langle \xi^2 \rangle L_0. \quad (3.12)$$

At this point all we need are the following averaged products

$$\langle \tilde{A}_{ey}(t)R(t) \rangle = -\kappa(t)\langle I(t) \rangle, \quad \langle \tilde{A}_{ey}(t)I(t) \rangle = \kappa(t)\langle R(t) \rangle. \quad (3.13)$$

These are derived from Eqs. (3.9) and (3.10) taking into account also (3.4), and are correct up to  $O(\kappa)$ . In terms of the averaged quantities defined as  $\langle P(t) \rangle = \mathcal{P}(\sqcup)$ ,  $\langle R(t) \rangle = \mathcal{R}(\sqcup)$ ,  $\langle I(t) \rangle = \mathcal{I}(\sqcup)$ , we can write the noise-averaged variant of the set (3.6) as:

$$\begin{aligned} \dot{\mathcal{P}}(t) &= 2H_{ey}\mathcal{I}(\sqcup) \\ \dot{\mathcal{R}}(t) &= -2A_{ey}(t)\mathcal{I}(\sqcup) - \epsilon\kappa(\sqcup)\mathcal{R}(\sqcup) \\ \dot{\mathcal{I}}(t) &= 2A_{ey}(t)\mathcal{R}(\sqcup) - \epsilon\kappa(\sqcup)\mathcal{I}(\sqcup) - \mathcal{H}_{\uparrow\ddagger}(\epsilon\mathcal{P}(\sqcup) - \infty). \end{aligned} \quad (3.14)$$

This system of equations explicitly exhibits the noise parameter  $\kappa$ <sup>4</sup>. Eliminating  $\mathcal{I}$  and  $\mathcal{R}$  from Eq. (3.14) we can obtain the following third order differential equation for the averaged conversion probability  $\mathcal{P}$ :

$$\begin{aligned} A_{ey}(t)\frac{d^3\mathcal{P}(\sqcup)}{dt^3} + [4\kappa(t)A_{ey}(t) - \dot{A}_{ey}(t)]\frac{d^2\mathcal{P}}{dt^2}(t) + [\omega_0^2(t)A_{ey}(t) + 2A_{ey}(t)\dot{\kappa}(t) \\ - 2\kappa(t)\dot{A}_{ey}(t)]\frac{d\mathcal{P}}{dt} - 4H_{ey}^2\mathcal{P}(\sqcup)(\mathcal{A}_{\uparrow\ddagger}(\sqcup) - \epsilon\kappa(\sqcup)\mathcal{A}_{\uparrow\ddagger}(\sqcup)) = \\ - 2H_{ey}^2(\dot{A}_{ey}(t) - 2\kappa(t)A_{ey}(t)), \end{aligned} \quad (3.15)$$

where the frequency  $\omega_0^2$  familiar from the MSW effect is given as

$$\omega_0^2(t) = 4(A_{ey}^2(t) + H_{ey}^2), \quad (3.16)$$

and the initial conditions become:

$$\mathcal{P}(\sqcup_l) = \infty, \quad \mathcal{P}'(\sqcup_l) = l, \quad \mathcal{P}''(\sqcup_l) = \epsilon\mathcal{H}_{\uparrow\ddagger}^\xi. \quad (3.17)$$

Let us notice that in the absence of noise ( $\kappa = 0$ ) the Eq. (3.15) reduces to the well known MSW equation (cfr. with (Eq. (2.23) of the first paper in Ref. [14]) with the change  $\bar{H} = 2H_{ey}$ ,  $H = 2A_{ey}$ ).

In order to gain some more insight on the present picture let us note that the MSW resonance condition, i.e.  $A_{ey}(t) = V_{ey}(t) - \Delta m^2 \cos 2\theta/2E = 0$ , remains unchanged, due to the random nature of the matter perturbations. In other words, the fact that the noise is a second order effect (see eq. (3.11)) means that it can only be seen in the conversion probability. In order to ensure that the correlation length  $L_0$  is smaller than the neutrino wave length

<sup>4</sup>These equations are equivalent to those obtained in Ref. [19] in terms of the variables  $x = 2\mathcal{R}$ ,  $y = -2\mathcal{I}$  and  $r = 2\mathcal{P} - \infty$ .

in the Sun, as required by the condition (2.7), we choose to adjust  $L_0$  as follows:

$$L_0 = 0.1 \times (\lambda_m) = 0.1 \times \frac{2\pi}{\omega_0}. \quad (3.18)$$

In order to get a feeling for the importance of the noise term in the system (3.14), note that the noise parameter  $\kappa$  in Eq. (3.12) is always smaller than  $A_{ey}(t)$ , for  $\xi \lesssim$  few %, except at the resonance region. As a result, the density perturbation can have its maximal effect just at the resonance. However, this is not enough for the noise to give rise to sizeable effects. Since the noise term gives rise to a damping term in the system (3.14), it follows that the corresponding noise length scale  $1/\kappa$  be much smaller than the thickness of the resonance layer  $\Delta r$ . In other words, it is also necessary that the following *adiabaticity* condition

$$\tilde{\alpha}_r = \Delta r \kappa_{res} > 1, \quad (3.19)$$

is satisfied. This condition is analogous to the standard MSW *adiabaticity* condition  $\alpha_r > 1$  where  $\alpha_r = \Delta r / (\lambda_m)_{res}$  is the standard adiabaticity parameter at resonance [14]. One can show that the two adiabaticity parameters are related as

$$\tilde{\alpha}_r \approx \alpha_r \frac{\xi^2}{\tan^2 2\theta}, \quad \alpha_r = \frac{\Delta m^2 \sin^2 2\theta R_0}{4\pi E \cos 2\theta}. \quad (3.20)$$

For the range of parameters we are considering,  $\xi \sim 10^{-2}$  and  $\tan^2 2\theta \geq 10^{-3} - 10^{-2}$ , and due to the restriction in the r.h.s of (2.7) one can estimate that  $\tilde{\alpha}_r \leq \alpha_r$ . Moreover, the relation  $\tilde{\alpha}_r \leq \alpha_r$  can be rewritten as  $\kappa_{res} < \delta H_r$ , where  $\delta H_r$  is the level splitting between the energies of the neutrino mass eigenstates at resonance. This shows that the energy perturbation induced by the matter fluctuations is not enough to cause the level crossing (even at the resonance) [17]. In other words, it never violates the MSW adiabaticity condition <sup>5</sup>.

From Eq. (3.20) it follows that, in the adiabatic regime  $\alpha_r > 1$ , the effect of the noise is larger the smaller the mixing angle value. Furthermore, as already noted above, Eq. (3.20) implies that the MSW non-adiabaticity  $\alpha_r < 1$  is always transmitted to  $\tilde{\alpha}_r < 1$ . As a result, under our assumptions the fluctuations are expected to be ineffective in the non-adiabatic MSW regime.

## 4. MSW Effect in Noisy Solar Matter

In this section we study the impact that random perturbations in the solar matter density can have upon the MSW solution to the solar neutrino problem. We will consider both the active to active and active to sterile neutrino conversion. For definiteness we will take as our reference SSM the most recent Bahcall-Pinsonneault (BP95) model with helium and heavy element diffusion, as given in the last paper in Ref. [8]. From there we will take both the electron (neutron) density as well as the neutrino energy spectra and

<sup>5</sup>This is opposite to the case of a local density jump as discussed by Krastev and Smirnov in the second paper in Ref. [17], where larger values of  $\delta\rho$  could break MSW adiabaticity.

detection cross sections. Using these as input, we have solved numerically the coupled differential equations in (3.14) for the  $\nu_e$  survival probability <sup>6</sup>.

In order to get some preliminary insight on the effect of the density noise, in Fig.1 we plot  $\mathcal{P}$  as a function of  $E/\Delta m^2$  for different values of the noise parameter  $\xi$ . For comparison, the standard MSW case  $\xi = 0$  is also shown (lower solid curve). We take this case as the reference situation with which all others with non-vanishing  $\xi$  are compared.

One concludes that in both cases of small and large mixing (Fig. 1a and Fig. 1b, respectively), the effect of the matter density noise is to weaken the MSW suppression in the adiabatic regime (see dotted and dashed curves) with negligible effect in the non-adiabatic region, in complete agreement with the results of Ref. [19]. The relative increase of the survival probability  $\mathcal{P}$  is larger for the case of small mixing (Fig. 1a) as already guessed on the basis of Eq. (3.20). One sees that the enhancement of the survival probability can easily reach 20% for  $\xi$  values as small as 4%. From these figures one can already infer that for the relevant  $\Delta m^2 \sim 10^{-5} \text{ eV}^2$  the intermediate energy neutrinos (like <sup>7</sup>Be neutrinos) are the ones most likely to be affected by the matter noise.

Note that the "white noise"-type density fluctuations we consider here cannot lead to any parametric enhancement [24] of the survival probability of the type discussed in Ref. [17] with a sinusoidal density perturbation. In contrast to that case, the effect of random perturbations is smooth, as suggested by the fact that the noise parameter  $\kappa$  plays the role of a friction term in Eq. (3.14).

Moreover, one can see from the figures that for the value  $E/\Delta m^2 \sim 6.7 \times 10^4 \text{ eV}^{-1} \cos 2\theta$ , required in order for the neutrinos to undergo resonant conversion just at the solar centre  $r = 0$ , the survival probability remains equal to 0.5 irrespective of the  $\xi$  values. The presence of this "fixed point" is easily understood: for such  $E/\Delta m^2$  value <sup>7</sup> the neutrino state  $|\nu_e \rangle = \sqrt{2}(|\nu_{1m} \rangle + |\nu_{2m} \rangle)/2$  is produced at its resonance point and  $\nu_{1m} \leftrightarrow \nu_{2m}$  transitions between matter eigenstates occur at the same rate. This case of coincidence of neutrino production point with its resonance point is the only one for which the effect of the matter noise is strictly absent, even if the adiabaticity condition holds.

## 5. Comparison with Solar Neutrino Experiments

As seen above, there can be a substantial effect of matter noise fluctuations on the neutrino conversion probabilities. It is therefore important to analyse the possible impact of this scenario in the determination of solar neutrino parameters from the experimental data. The most recent averaged data of

<sup>6</sup>For simplicity and CPU economy we have not included throughout our analysis the neutrino production distributions in the Sun.

<sup>7</sup>Note that the matter mixing angle is understood as the mixing angle that diagonalises the Hamiltonian Eq. (3.2) at each time  $t$ . It is written as  $\sin^2 2\theta_m = 4H_{ex}^2/\omega_0^2$ . At resonance  $\omega_0^2 = 4H_{ex}^2$ , so that  $\sin^2 2\theta_m = 1$ .

the chlorine [1], gallium [2,3] and Kamiokande [4] experiments are:

$$R_{Cl}^{exp} = (2.55 \pm 0.25)\text{SNU}, \quad R_{Ga}^{exp} = (74 \pm 8)\text{SNU}, \quad R_{Ka}^{exp} = (0.44 \pm 0.06)R_{Ka}^{BP95} \quad (5.1)$$

where  $R_{Ka}^{BP95}$  is the BP95 SSM prediction. For the gallium result we have taken the of GALLEX  $R_{Ga}^{exp} = (77 \pm 8 \pm 5)\text{SNU}$  [2] and SAGE  $R_{Ga}^{exp} = (69 \pm 11 \pm 6)\text{SNU}$  [3] measurements. The detection rates in the chlorine and gallium experiments are given as

$$R_{Cl,Ga} = \int dE \sigma(E) \mathcal{P}(\mathcal{E}) \sum_{\nu_i} \phi_{\nu_i}(\mathcal{E}), \quad (5.2)$$

where the sum is understood over the  $\nu$  source contributions ( $i = {}^7\text{Be}, {}^8\text{B} \dots$ ) and  $\sigma(E)$  are the corresponding neutrino cross sections. For the Kamiokande experiment, the detection rate is

$$R_k = \int_{Th} dE [\sigma_{\nu_e}(E) \mathcal{P}(\mathcal{E}) + \sigma_{\nu_s}(\mathcal{E})(\infty - \mathcal{P}(\mathcal{E}))] \phi_B(\mathcal{E}), \quad (5.3)$$

where  $\sigma_{\nu_e}(E)$  and  $\sigma_{\nu_x}(E)$  ( $x = \mu, \tau$ ) are the  $\nu_e - e$  and  $\nu_x - e$  elastic scattering cross sections, respectively, and 'Th' stands for the detection energy threshold. In the case of sterile conversion  $\sigma_{\nu_x} = 0$ .

In Fig. 2 we show the iso-signal contours (within  $2\sigma$  standard deviations) for each experiment and for different  $\xi$  values. These plots demonstrate that the horizontal adiabatic lines are the ones mostly affected by the noise fluctuations. Indeed, the larger the  $\xi$  value, the greater the suppression of the neutrino conversion and, as a result, the larger the shift of this horizontal branch towards smaller  $\Delta m^2$  values. These lower  $\Delta m^2$  values allow neutrinos of lower energy to be involved in the adiabatic conversion (since the resonance matter density is proportional to  $\Delta m^2/E$ ) so as to compensate for the effect of the matter noise. Notice also that, because of this downward shift in  $\Delta m^2$ , the minimum allowed values of  $\sin^2 2\theta$  for each experiment becomes larger in order to preserve adiabaticity (see Eq. (3.20)). Also the diagonal (so-called "non-adiabatic") and the upper portion of the vertical (so-called large mixing) branches of the MSW plot are modified by the effect of noise. The diagonal lines are deformed mostly in the upper-left part, due to a shift of the kink towards larger values of the mixing angle. In contrast, they are less affected for  $\sin^2 2\theta \gtrsim 10^{-2}$ . This follows from the fact that for larger mixing the noise adiabaticity is lost (see Eq.(3.20)). Thus we find that the expectations derived on the basis of our discussion in the previous section are confirmed.

Comparing the allowed regions of all experiments shown in Fig. 2a, 2b and 2c for the  $\nu_e \rightarrow \nu_\mu$  or  $\nu_\tau$  neutrino conversion case, one concludes that the overlapping area is not substantially changed in the small mixing branch, whereas it increases in the adiabatic one, for large mixing  $\sin^2 2\theta > 0.3$  and  $10^{-5}\text{eV}^2 < \Delta m^2 < 10^{-4}\text{eV}^2$ .

We now turn to the case of  $\nu_e \rightarrow \nu_s$  sterile resonant transitions. Here the  $\nu_e$  survival probability is not substantially changed with respect to the active neutrino conversion case, since the solar neutron contribution in the matter potential is rather small, compared to that of the electrons. As a result the signal expected in radiochemical experiments is rather insensitive to whether the converted neutrino is active or sterile. Thus we focus on the Kamiokande

experiment. In Fig. 2d we show the iso-signal contours for the case of sterile neutrino conversion. One can see from the figure that in the sterile case, irrespective of the assumed level of noise, the vertical large mixing branch gets thinner and closer to the maximal mixing region  $\sin^2 2\theta = 1$ . This is required, of course, in order to increase the contribution to the signal which is now lost when compared to the active  $\nu_{\mu,\tau}$  case. One can also see that the noise has the same qualitative features as in the case of active conversions, mostly affecting the horizontal adiabatic region of larger  $\Delta m^2$ .

In order to determine the solar neutrino parameters  $\Delta m^2$  and  $\sin^2 2\theta$  we now proceed to perform a  $\chi^2$  analysis for the present experimental data. For simplicity we neglect for the moment the theoretical uncertainties.

The results of our fit are shown in Fig. 3, where the 90% confidence level (C.L) areas are drawn for different  $\xi$  values (see also Table 1). From Fig. 3a one can observe the modifications in the small mixing region caused by the noise in the case of active neutrino conversion. One sees that there is a slight shift of  $\Delta m^2$  towards lower values and a larger shift of  $\sin^2 2\theta$  towards larger values. For example the allowed region for the mixing angle covers the range  $4 \times 10^{-3} < \sin^2 2\theta < 8 \times 10^{-3}$  obtained for  $\xi = 0$  becomes  $8 \times 10^{-3} < \sin^2 2\theta < 2 \times 10^{-2}$  for  $\xi = 8\%$ . The corresponding allowed  $\Delta m^2$  range is  $2.5 \times 10^{-6} < \Delta m^2 < 9 \times 10^{-6} \text{ eV}^2$  to be compared with  $5 \times 10^{-6} < \Delta m^2 < 1.2 \times 10^{-5} \text{ eV}^2$  in the noiseless case. The large mixing area is less stable, exhibiting a tendency to shift towards smaller  $\Delta m^2$  and  $\sin^2 2\theta$ . For example, if we take  $\xi = 8\%$ , for the sake of argument, we find that the small mixing region is much more stable than the large mixing one, even for such a relatively large value of the noise.

As for the value of the minimal  $\chi^2$ , the presence of the matter density noise makes the data fit a little poorer:  $\chi_{min}^2 = 0.1$  for  $\xi = 0$ ,  $\chi_{min}^2 = 0.8$  for  $\xi = 4\%$  and  $\chi_{min}^2 = 2.1$  for  $\xi = 8\%$ . Also the best fit points where the  $\chi_{min}^2$  is achieved change slightly: the value of  $\Delta m^2 \sim 6 \div 7 \times 10^{-6} \text{ eV}^2$  is almost unchanged, while the value of the mixing angle gets larger with respect to the noiseless case. For example,  $\sin^2 2\theta = 6 \times 10^{-3}$  for  $\xi = 0$  while  $\sin^2 2\theta = 8 \times 10^{-3}$  for  $\xi = 4\%$  and  $\sin^2 2\theta = 10^{-2}$  for  $\xi = 8\%$ . The strong  ${}^7\text{Be}$  neutrino suppression, characteristic of the MSW effect, is reduced by the presence of matter noise (see Fig. 1). As a result, the conflict between chlorine and Kamiokande data is exacerbated and the data fit gets worse. In any case our results for  $\chi_{min}^2$  (see Table 1) indicate that the MSW scenario still provides a good fit of the totality of solar neutrino data, even in the presence of matter fluctuations, as long as  $\xi \leq 8\%$  or so.

As for the large mixing solution, although the  $\chi_{min}^2$  value is not substantially changed with respect to the noiseless case (see Table 1A), we find that it acquires an increased statistical significance with respect to the corresponding region of the noiseless case. Our results show that the large mixing solution gets wider than in the noiseless case. For example the smallest allowed  $\sin^2 2\theta$  value shifts from  $\sin^2 2\theta \sim 0.4$  for  $\xi = 4\%$  down to  $\sin^2 2\theta \sim 7 \times 10^{-2}$  for  $\xi = 8\%$ .

As for the best fit points we find that  $\Delta m^2 \sim 10^{-5} \text{ eV}^2$  is almost unchanged, whereas the best value of the mixing angle decreases from  $\sin^2 2\theta = 0.67$  for the noiseless case down to  $\sin^2 2\theta = 0.27$  for  $\xi = 8\%$ . Note that the possibility of lowering the mixing angle value  $\sin^2 2\theta$  characterising the large mixing MSW solution in the presence of noise may eliminate the super-

nova argument given in Ref. [25] against such solution. In agreement with Ref. [13], we find that in our fit this region appears already at the 80% C.L. in the  $\xi = 0$  case <sup>8</sup>.

We now turn to the case of sterile solar neutrino conversions. We find that the data fit is worse ( $\chi_{min}^2 = 1$ ) than for the active case (see Fig. 3b and Table 1B) and it excludes, even at 95% C.L., the large mixing region (in the noiseless case). This is in agreement with previous analyses [15,13]. However, the presence of matter density noise may restore this region. For example for  $\xi = 8\%$ , although the data fit is much worse than in the  $\xi = 0$  case, the large mixing region appears at the 90% C.L. We may note in this context that the indicated range for the mixing angle is not in conflict with the primordial helium abundance constraints [26].

So far in our analysis we have neglected SSM theoretical uncertainties, and worked entirely within the BP95 model [8]. One way to account for these uncertainties would be to allow the solar neutrino fluxes to vary as suggested in Ref. [16,12]. However one can get an idea (even if partial) of these uncertainties by simply repeating the data fit assuming the SSM of Turck-Chieze *et al.* (TCL) [9]. For our purposes the main difference between this model and the BP95 model is that it predicts a lower <sup>8</sup>B flux. The comparison of the allowed parameter regions obtained in the framework of the TCL model, Fig. 3 (c,d), with those obtained using the BP95 model, Fig. 3 (a,b), shows that the general features of the effect of the noise are maintained. In particular, our results once again establish the fact that the indicated  $\Delta m^2$  range for the small mixing MSW solution is fairly stable, as long as the assumed noise level is not too large. Note also from the figures that, even though the effect of the noise is to lower the  $\Delta m^2$  range for the large mixing solution, the region obtained (e.g. for  $\xi = 8\%$ ) lies higher than the corresponding range for the BP95 model.

## 6. Implications for Future Experiments

Up to now we have discussed the possible consequences of the presence of matter fluctuations for the ongoing solar neutrino experiments. We now turn our attention to the possibility of probing the level of matter noise in the Sun in the next generation of solar neutrino experiments.

As we have seen the <sup>7</sup>Be neutrinos are the component of the solar neutrino spectrum which is most affected by the presence of matter noise. Therefore the future Borexino experiment, aimed to detect the <sup>7</sup>Be neutrino flux [27] through the elastic  $\nu - e$  scattering should be an ideal tool for studying the solar matter fluctuations.

In Ref. [15] it was shown that in the relevant (noiseless) MSW parameter region the Borexino signal cannot be sharply predicted. This is illustrated in Fig. 4a, where we display the Borexino signal in the  $\Delta m^2 - \sin^2 2\theta$  plane, expressed in units of the expected SSM rate, i.e.  $Z_{Be} = R_{Be}^{pred} / R_{Be}^{SSM}$ . As one can see, the allowed range for the signal in this case lies anywhere between 0.2 to 0.7 of the SSM prediction. In Fig. 4b, we show the corresponding beryllium line predictions for the case of noisy MSW, assuming  $\xi = 4\%$ .

---

<sup>8</sup>This result may be underestimated since the earth regeneration effect has not been included.

We see that the presence of matter noise strongly modifies the picture: the minimal allowed value for  $Z_{Be}$  now becomes higher,  $Z_{Be} \geq 0.37$ . Therefore if the Borexino experiment detects a small signal,  $Z_{Be} \lesssim 0.3$  (with sufficient accuracy) this will imply that a 4% level of matter fluctuations in the central region of the Sun is rather unlikely to be present if the MSW mechanism is responsible for the explanation of the solar neutrino deficit <sup>9</sup>.

Note, on the other hand, that if a higher value  $Z_{Be} \gtrsim 0.5$  would be found experimentally, this would be incompatible with the small mixing MSW solution with noise at the  $\xi = 4\%$  level. However, this higher signal could be consistent with the both the large mixing MSW solution as well as the noiseless small angle MSW solution. On the other hand, if the noise level is higher,  $\xi = 8\%$ , the allowed  $Z_{Be}$  range narrows down to values between 0.5 to 0.65.

Let us turn to the case sterile resonant conversion in the noisy MSW effect. Let us imagine that future large detectors such as Super-Kamiokande and/or the Sudbury Neutrino Observatory (SNO) establish through, e.g. the measurement of the charged to neutral current ratio, that the deficit of solar neutrinos is due to the  $\nu_e \rightarrow \nu_s$  resonant conversion. In this case, the minimum signal expected in Borexino is very small  $Z_{Be} \approx 0.02$  for  $\xi = 0$  (see Fig. 4c). On the other hand in the noisy case with  $\xi = 4\%$ , the minimum expected Borexino signal is 10 times higher than in the noiseless case, so that if Borexino detects a rate  $Z_{Be} \lesssim 0.1$  (see Fig. 4d) this would again exclude noise levels above 4%.

## 7. Discussion and Conclusions

We have presented a comprehensive study of the effects of the matter density noise upon the MSW solution to the solar neutrino problem. We have adopted the wave function Schrödinger formalism to re-write the corresponding MSW evolution equations for the neutrino survival probabilities. The fluctuations weaken the efficiency of the MSW suppression in the adiabatic regime, whereas they are much less effective in the non-adiabatic regime. In our data fit we have shown that the MSW solution still exists for realistic levels of matter density noise  $\xi \lesssim 8\%$ . However, our  $\chi^2$  analysis has shown that the quality of the fit gets a little worse if these noisy matter perturbations are present. In any case the mass range determined from our fit for the small mixing MSW solution  $4 \times 10^{-6} \text{eV}^2 < \Delta m^2 < 10^{-5} \text{eV}^2$  is relatively stable at 90% C.L., whereas the mixing angle determination appears more sensitive to the assumed level of fluctuations, and shifts  $\sin^2 2\theta$  towards larger values up to  $10^{-2}$ . These trends also hold for the case of sterile solar neutrino conversion. In the latter case we have found that in the presence of solar density noise the large mixing region gets somewhat improved statistical significance when compared with the noiseless case. However, it remains highly disfavoured with respect to the small mixing MSW solution.

We have also explored the potential of the Borexino experiment to "test" the level of matter density fluctuations in the solar interior through the mea-

---

<sup>9</sup>In principle any value of  $Z_{Be}$  is also compatible with the just-so oscillation scenario [12,13], but here the strong seasonal <sup>7</sup>Be and *pep* signal variations, would help to distinguish from the MSW case.

surement of the  ${}^7\text{Be}$  neutrino flux, as depicted in Fig. 4.

Finally, we note that in our analysis we have neglected the details of the neutrino production distribution as a function of the distance to the solar centre. It is well known that this affects mainly the low energy  $pp$  neutrinos [14]. As a result, the iso-signal curves we have obtained for the gallium experiments are somewhat less reliable in the position of the kink corresponding to  $\Delta m^2 \lesssim 2 \times 10^{-6} \text{eV}^2$  marking the onset of  $pp$  neutrino suppression and lying on the gallium non-adiabatic branch. However, this does not substantially affect the determination of the relevant regions where *all* solar neutrino data are explained through the MSW effect. This includes both small as well as large mixing MSW solutions.

## Acknowledgements

We thank Z. Berezhiani, N. Hata P. Krastev, S. Mikheyev and A. Smirnov for valuable comments and discussion. We also thank S. Turck-Chi eze for an informative conversation. This work has been supported by DGICYT under Grant numbers PB92-0084, SAB94-0325 and by RFFR-95-02-03724 (V. S.), by the grant N. ERBCHBI CT-941592 of the Human Capital and Mobility Program (A. R.) and by a DGICYT postdoctoral fellowship (H. N.)

<b>A: active</b>	$\xi = 0$	$\xi = 2\%$	$\xi = 4\%$	$\xi = 8\%$
small $\theta$				
$\chi_{min}^2$	0.10	0.23	0.80	2.1
$\Delta m^2(10^{-5}\text{eV}^2)$	0.68	0.71	0.65	0.61
$\sin^2 2\theta$	$6.2 \times 10^{-3}$	$7.3 \times 10^{-3}$	$7.5 \times 10^{-3}$	$10^{-2}$

large $\theta$				
$\chi_{min}^2$	3.3	2.9	3.0	3.2
$\Delta m^2(10^{-5}\text{eV}^2)$	2.7	2.4	2.0	1.2
$\sin^2 2\theta$	0.67	0.69	0.57	0.27

<b>B: sterile</b>	$\xi = 0$	$\xi = 2\%$	$\xi = 4\%$	$\xi = 8\%$
small $\theta$				
$\chi_{min}^2$	1.0	1.9	3.6	8.9
$\Delta m^2(10^{-5}\text{eV}^2)$	0.53	0.50	0.49	0.40
$\sin^2 2\theta$	$7.5 \times 10^{-3}$	$7.5 \times 10^{-3}$	$9.0 \times 10^{-3}$	$1.3 \times 10^{-2}$

large $\theta$				
$\chi_{min}^2$	10	11	11	11
$\Delta m^2(10^{-5}\text{eV}^2)$	1.4	1.2	1.6	1.0
$\sin^2 2\theta$	0.83	0.83	0.69	0.39

**Table 1.** The values of  $\chi_{min}^2$ , for 1 degree of freedom, and the corresponding best fit  $\Delta m^2$  and  $\sin^2 2\theta$  parameters in the small and large mixing regions, for different values of  $\xi$ . Tables **A** and **B** are for the active-active and active-sterile conversion respectively, using the latest 1995 Bahcall-Pinsonneault (BP95) model.

<b>A:</b> <i>active</i>	$\xi = 0$	$\xi = 2\%$	$\xi = 4\%$	$\xi = 8\%$
small $\theta$				
$\chi_{min}^2$	0.10	0.46	1.1	3.0
$\Delta m^2(10^{-5}\text{eV}^2)$	0.64	0.66	0.62	0.66
$\sin^2 2\theta$	$3.6 \times 10^{-3}$	$3.6 \times 10^{-3}$	$4.3 \times 10^{-3}$	$5.2 \times 10^{-3}$

large $\theta$				
$\chi_{min}^2$	5.2	5.2	5.0	4.3
$\Delta m^2(10^{-5}\text{eV}^2)$	17	16	12	3.8
$\sin^2 2\theta$	0.83	0.83	0.83	0.69

<b>B:</b> <i>sterile</i>	$\xi = 0$	$\xi = 2\%$	$\xi = 4\%$	$\xi = 8\%$
small $\theta$				
$\chi_{min}^2$	0.69	2.1	2.3	5.6
$\Delta m^2(10^{-5}\text{eV}^2)$	0.51	0.45	0.48	0.57
$\sin^2 2\theta$	$4.3 \times 10^{-3}$	$4.2 \times 10^{-3}$	$5.2 \times 10^{-3}$	$6.3 \times 10^{-3}$

large $\theta$				
$\chi_{min}^2$	9.3	9.3	9.2	8.3
$\Delta m^2(10^{-5}\text{eV}^2)$	16	15	14	3.3
$\sin^2 2\theta$	0.83	0.83	0.83	0.69

**Table 2.** The same as for Table 1, but using the Turck-Chieze *et al.* (TCL) SSM.

## Figure Captions

### Fig. 1.

Averaged solar neutrino survival probability  $\mathcal{P}$  versus  $E/\Delta m^2$  for small mixing (a:  $\sin^2 2\theta = 10^{-2}$ ) and large mixing (b:  $\sin^2 2\theta = 0.7$ ). The solid, dotted, dashed and dot-dashed curves correspond to noise levels  $\xi = 0, 2\%, 4\%$  and  $8\%$ , respectively.

### Fig. 2.

Iso-rate contours for the chlorine (a), gallium (b) and  $\nu - e$  scattering (c) experiments for the case of active neutrino conversion,  $\nu_e \rightarrow \nu_{\mu,\tau}$ . The threshold energy for the recoil electron detection is 7.5 MeV. For the radiochemical experiments the results are in SNU, whereas for the  $\nu - e$  scattering experiment these are given in units of the BP95 SSM prediction. The contours delimit the  $2\sigma$  allowed regions. The solid, dashed and dotted curves correspond to  $\xi = 0, 4\%$  and  $8\%$ , respectively. Fig. 2d gives the same iso-rate contours for the case of sterile  $\nu_e \rightarrow \nu_s$  conversion for the  $\nu - e$  scattering experiment.

### Fig. 3.

The 90% C.L. allowed regions (given by the condition  $\chi^2 \leq \chi_{min}^2 + 4.61$ ) for the active (a and c) conversion and for the sterile (b and d) conversion. For Fig. 3a and 3b, the C.L. allowed regions are obtained using the most recent Bahcall and Pinsonneault (BP95) SSM; for Fig. 3c and 3d we used the Turck-Chieze and Lopes (TCL) SSM. In Fig. 3a, 3b, 3c and 3d the solid, dot, dash, dot-dash curves correspond to the cases  $\xi = 0, 2\%, 4\%$  and  $8\%$ , respectively. The  $\chi_{min}^2$  and the corresponding  $(\Delta m^2, \sin^2 2\theta)$  best fit points are given in Table 1 and Table 2.

### Fig. 4.

The iso-signal contours of the ratio  $Z_{Be} = R_{Be}^{pred}/R_{Be}^{SSM}$  (figures at the curves) in the  $\nu - e$  scattering Borexino detector (solid lines). The threshold energy for the recoil electron detection is 0.25 MeV. The 90% C.L. allowed regions (dotted lines) and the corresponding best fit points (diamonds) are also superimposed, as determined by the present experimental data and using the BP95 SSM.

The case of active resonant conversion is presented in Fig. 4a and Fig. 4b for  $\xi = 0$  and  $\xi = 4\%$ , respectively. Analogously, Fig. 4c ( $\xi = 0$ ) and Fig. 4d ( $\xi = 4\%$ ) refer to the case of sterile neutrino resonant conversion.

## References

- [1] B.T. Cleveland *et al.*, *Nucl. Phys. B (Proc. Suppl.)* **38** (1995) 47.
- [2] GALLEX Collaboration, P. Anselmann *et al.*, LNGS Report 95/37 (June 1995).
- [3] SAGE Collaboration, J.S. Nico *et al.*, *Proc. 27th Conf. on High Energy Physics*, Glasgow, UK (July 1994).
- [4] Y. Suzuki, *Nucl. Phys. B (Proc. Suppl.)* **B38** (1995) 54
- [5] For a review see A. Yu. Smirnov, *Elementary Particle Physics: Present and Future*, proceedings of the International Workshop held in Valencia in June 1995, to be published by World Scientific (eds. A. Ferrer and J. W. F. Valle).
- [6] V. Castellani, *et al Phys. Lett.* **B324** (1994) 245;  
N. Hata, S. Bludman, and P. Langacker, *Phys. Rev.* **D49** (1994) 3622;  
V. Berezinsky, Comments on Nuclear and Particle Physics **21** (1994) 249;  
J. N. Bahcall, *Phys. Lett.* **B338** (1994) 276.
- [7] V. Berezinsky, G. Fiorentini and M. Lissia, preprint LGNS-95/96, INFNFE-15-95, INFNCA-TH9511.
- [8] J. N. Bahcall and R. K. Ulrich, *Rev. Mod. Phys.* **60** (1990) 297;  
J. N. Bahcall and M. H. Pinsonneault, *Rev. Mod. Phys.* **64** (1992) 885; J. N. Bahcall and M. H. Pinsonneault, preprint IASSNS-AST 95/24
- [9] S. Turck-Chiéze and I. Lopes, *Ap. J.* **408** (1993) 346;  
S. Turck-Chiéze *et al.*, *Phys. Rep.* **230** (1993) 57.
- [10] V. Castellani, S. Degl'Innocenti and G. Fiorentini, *Astron. Astrophys.* **271** (1993) 601.
- [11] P. I. Krastev and S. T. Petcov, preprint IASSNS-AST 95/40, SISSA 9/95/EP (hep-ph 9510367).
- [12] Z. Berezhiani and A. Rossi, *Phys. Rev.* **D51** (1995) 5229; preprint INFN FE-12-95, FTUV/95-55, IFIC/95-577 (hep-ph/9507393)
- [13] E. Calabresu *et al.*, preprint INFNFE-10-95, INFNCA-TH9512;  
J. N. Bahcall and P. I. Krastev, Princeton preprint IASSNS-AST 95/56, hep-ph/9512378
- [14] S. P. Mikheyev and A. Yu. Smirnov, *Sov. J. Nucl. Phys.* **42** (1986) 913; *Sov. Phys. Usp.* **30** (1987) 759;  
L. Wolfenstein, *Phys. Rev.* **D17** (1978) 2369; *ibid.* **D20** (1979) 2634.
- [15] G. Fiorentini *et al. Phys. Rev.* **D49** (1994) 6298;  
N. Hata and P. Langacker, *Phys. Rev.* **D50** (1994) 632.
- [16] P. I. Krastev and A. Yu. Smirnov, *Phys. Lett.* **B338** (1994) 282;  
V. Berezinsky, G. Fiorentini and M. Lissia, *Phys. Lett.* **B341** (1994) 38.
- [17] P. I. Krastev and A. Yu Smirnov, *Phys. Lett.* **B226** (1989) 341; *Mod. Phys. Lett.* **A6** (1991) 1001.
- [18] A. Schafer and S. E. Koonin, *Phys. Lett.* **B185** (1987) 417;  
R. F. Sawyer, *Phys. Rev.* **D42** (1990) 3908;  
A. Abada and S.T. Petcov, *Phys. Lett.* **B279** (1992) 153.

- [19] F. N. Loreti and A. B. Balantekin, *Phys. Rev.* **D50** (1994) 4762.
- [20] J. T. Peltoniemi, D. Tommasini, and J. W. F. Valle, *Phys. Lett.* **B298** (1993) 383; J. T. Peltoniemi, and J. W. F. Valle, *Nucl. Phys.* **B406** (1993) 409; D. O. Caldwell and R. N. Mohapatra, *Phys. Rev.* **D48** (1993) 3259; A. S. Joshipura and J. W. F. Valle, *Nucl. Phys.* **B440** (1995) 647.
- [21] P. Kumar, E. Quataert, and J. N. Bahcall, astro-ph/9512091
- [22] J. Christensen-Dalsgaard, private communication.
- [23] I. A. Akhiezer, R. V. Polovin, A. G. Sitenko and K. N. Stepanov, *Plasma Electrodynamics*, Volume 2. Non-linear Theory and Fluctuations, Pergamon Press, Oxford. New-York. Toronto Sydney. Paris. Braunschweig, 1975, p. 131.
- [24] L. D. Landau and E. M. Lifshitz, *Mechanics* vol. 1, p. 80, Pergamon Press, Oxford (1960).
- [25] A. Yu. Smirnov, D. N. Spergel and J. N. Bahcall, *Phys. Rev.* **D49** (1994) 1389.
- [26] See e.g. X. Shi, D. N. Schramm, B. D. Fields, *Phys. Rev.* **D48** (1993) 2563
- [27] C. Arpesella *et al.* (Borexino Collaboration), Proposal of BOREXINO (1991).

Fig. 1a

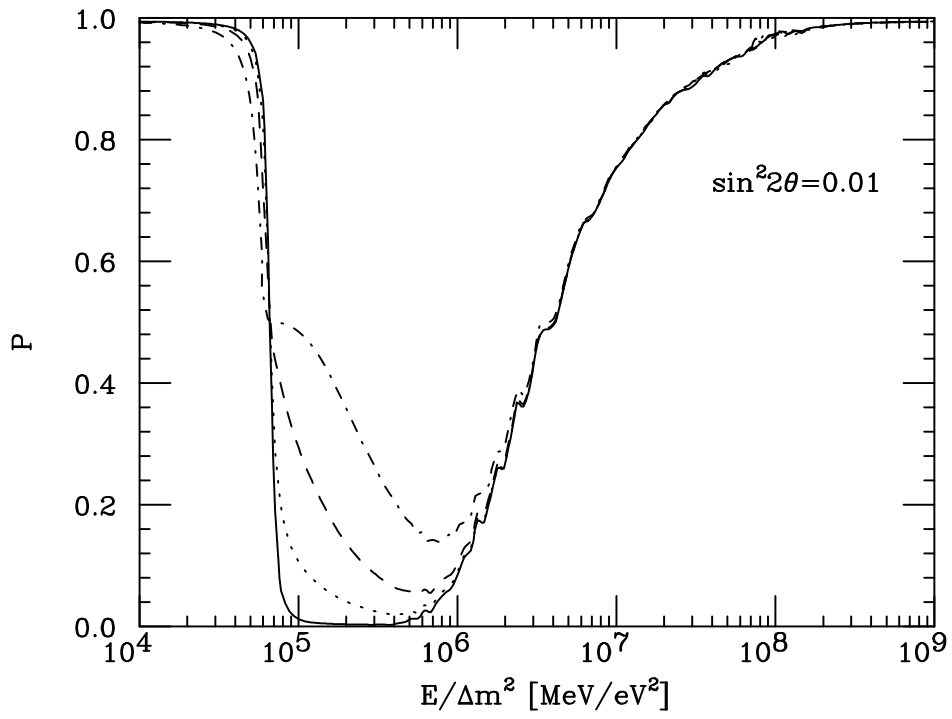


Fig. 1b

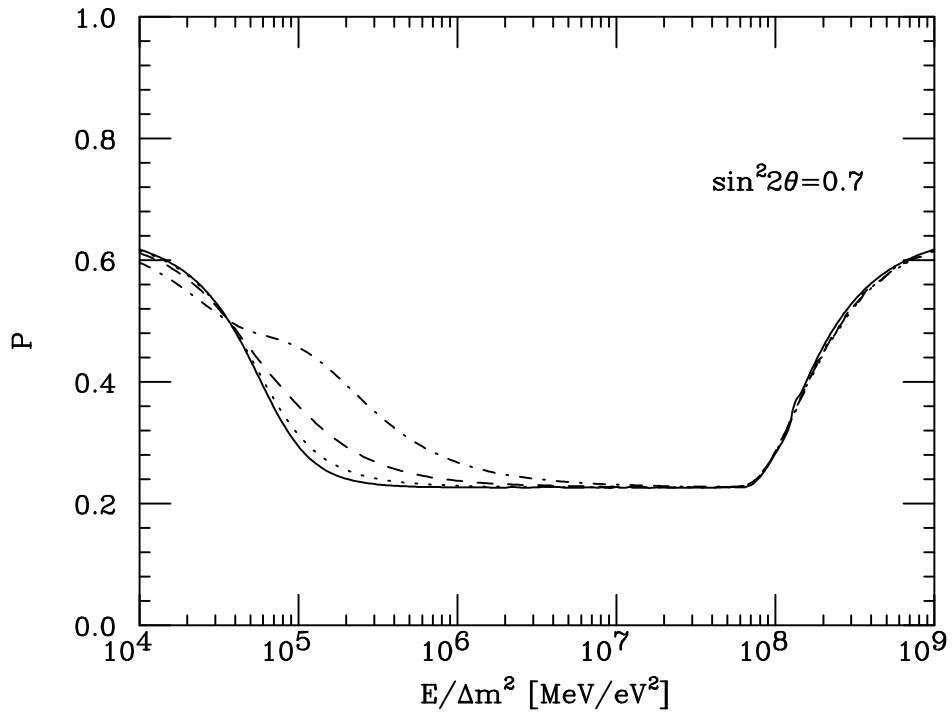


Fig. 2a

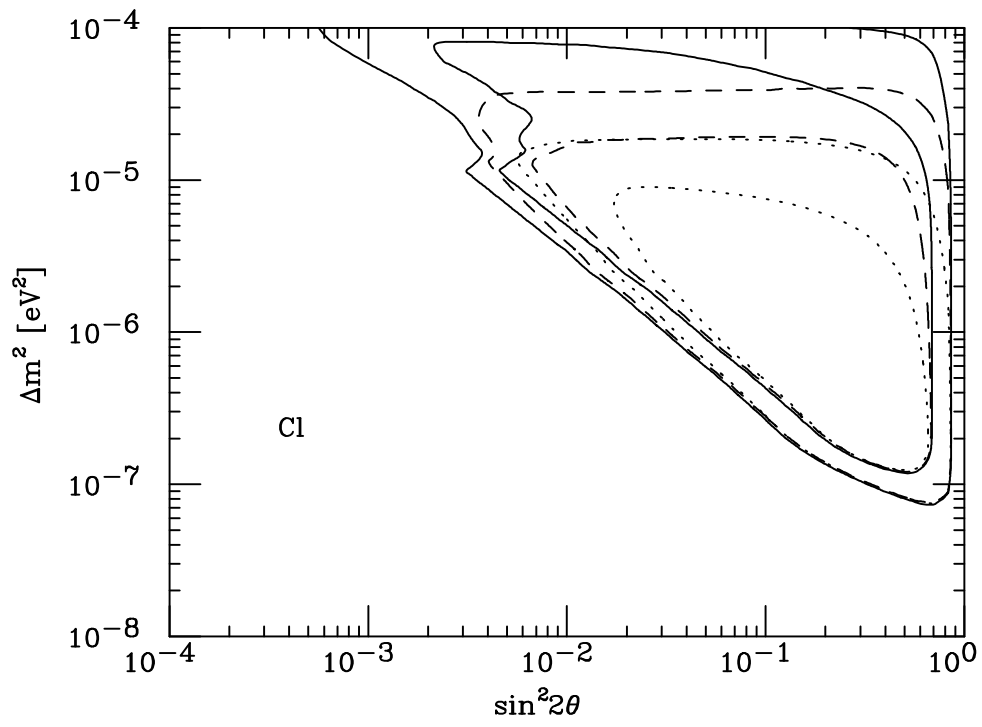


Fig. 2b

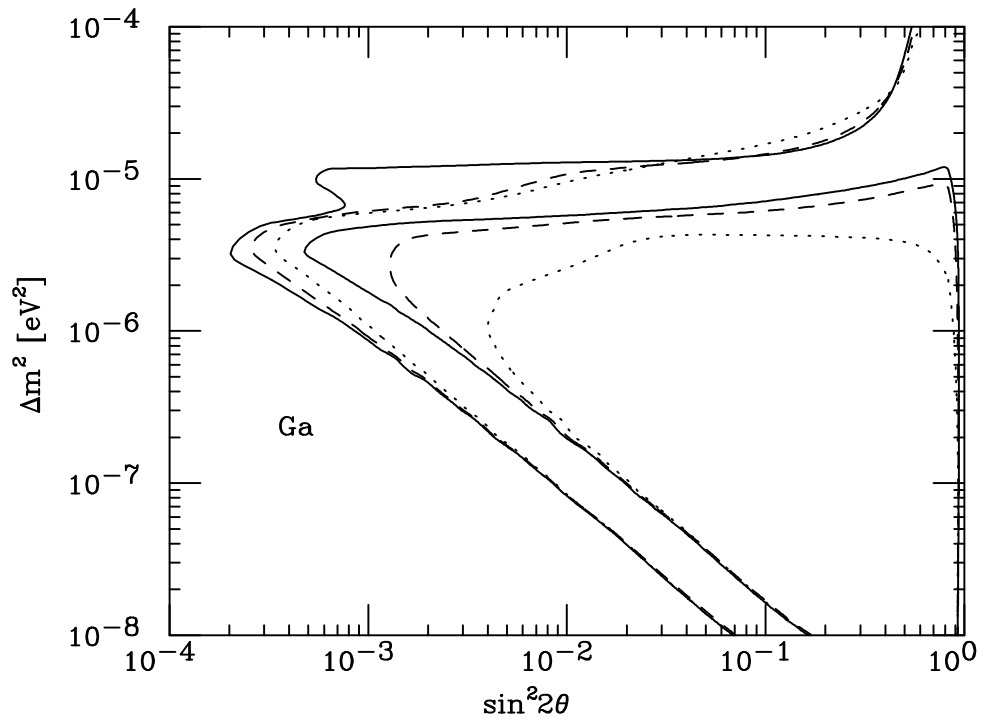


Fig. 2c

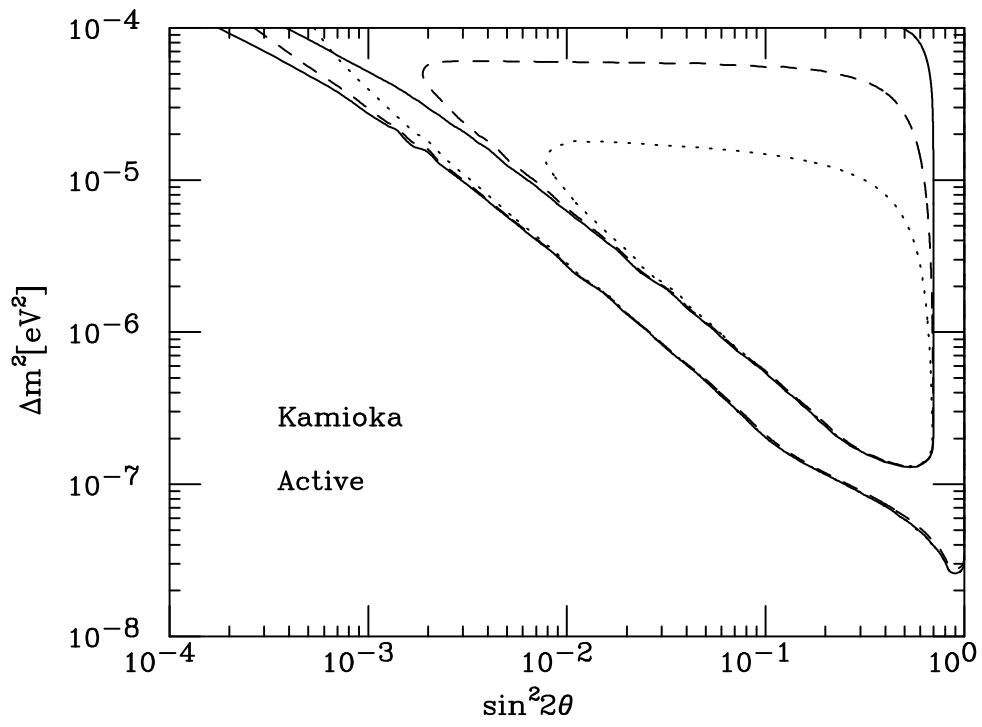


Fig. 2d

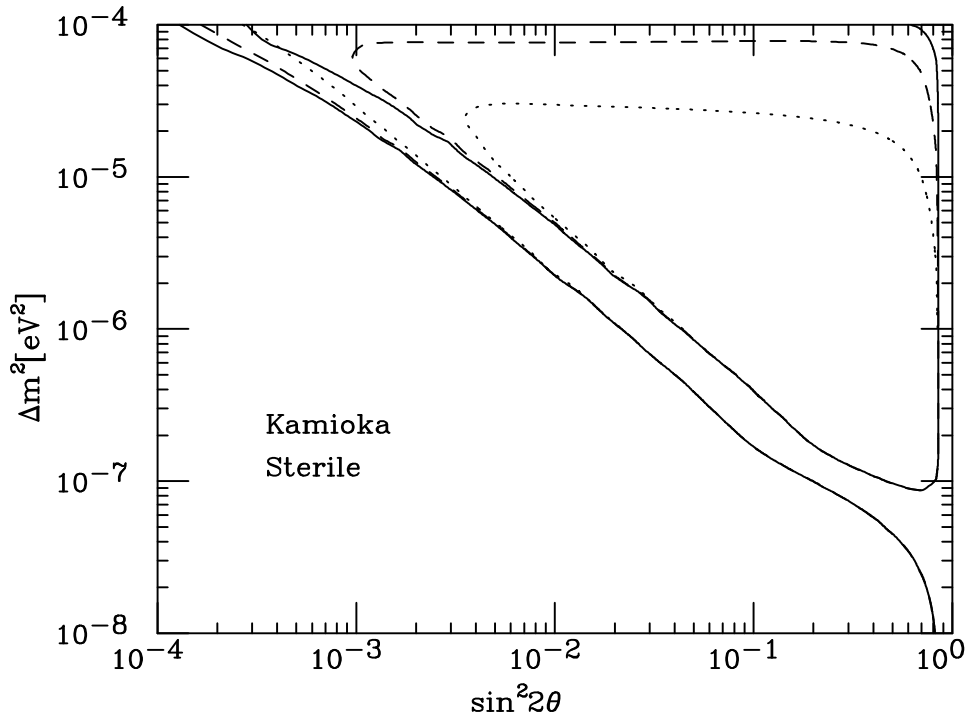


Fig. 3a

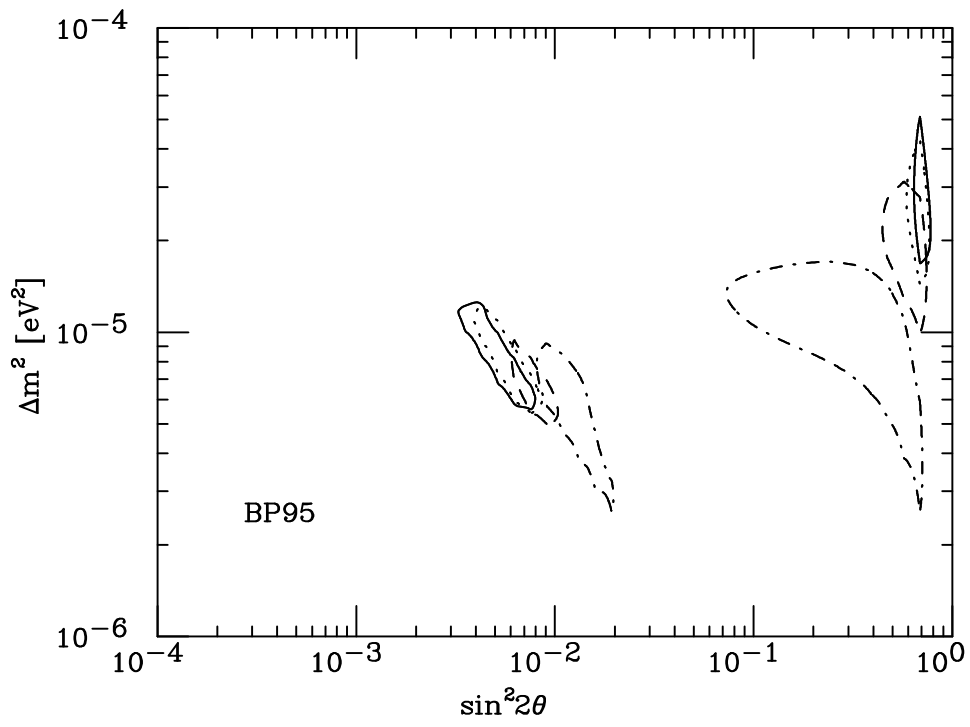


Fig. 3b

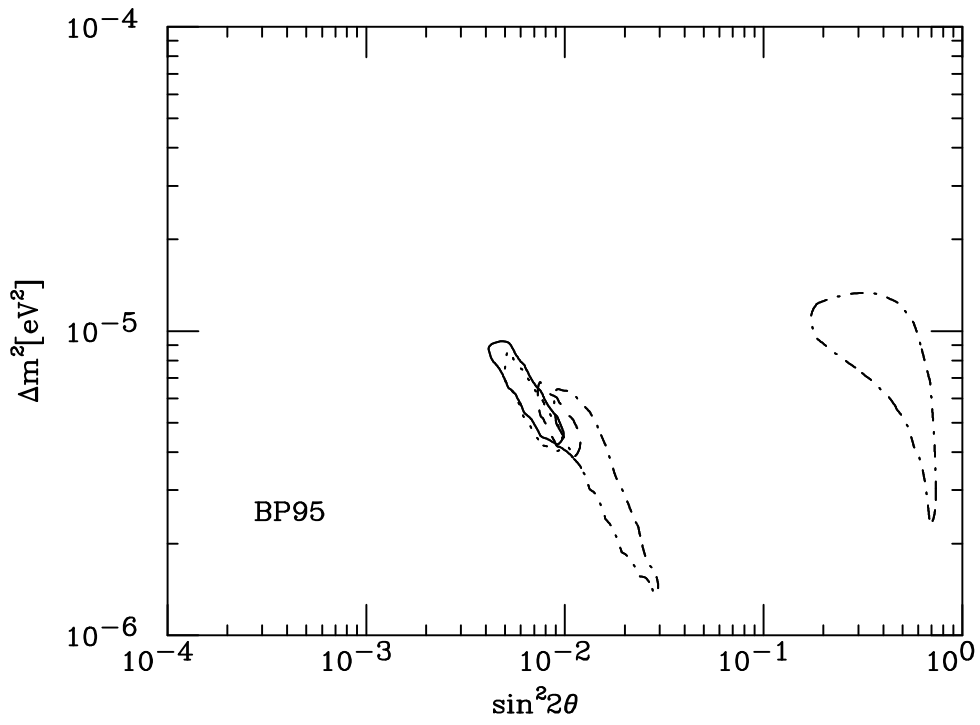


Fig. 3c

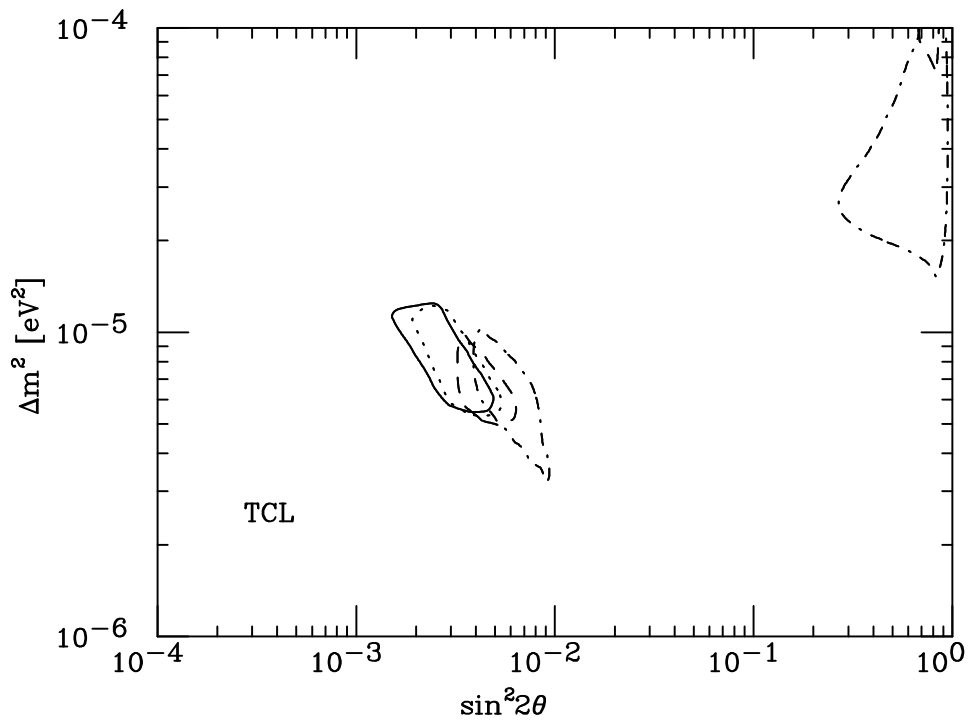


Fig. 3d

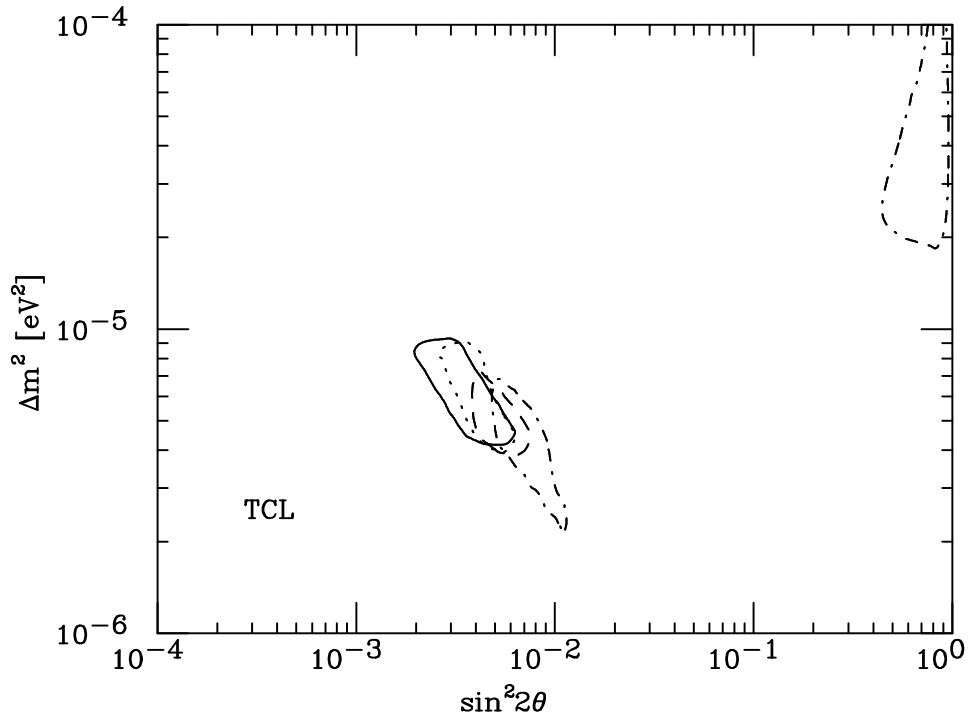


Fig. 4a

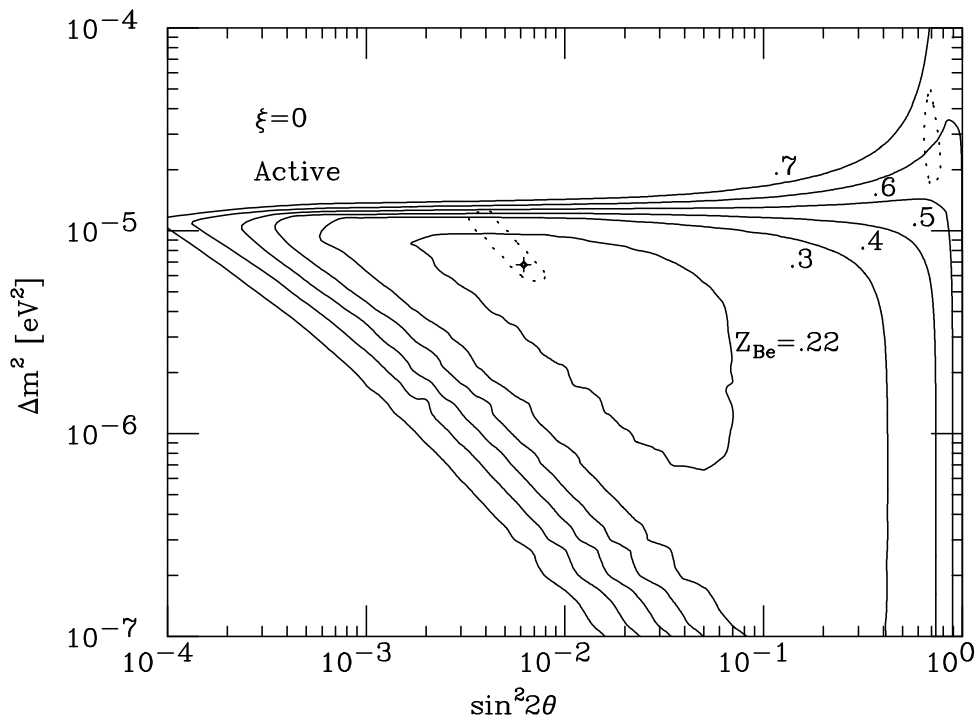


Fig. 4b

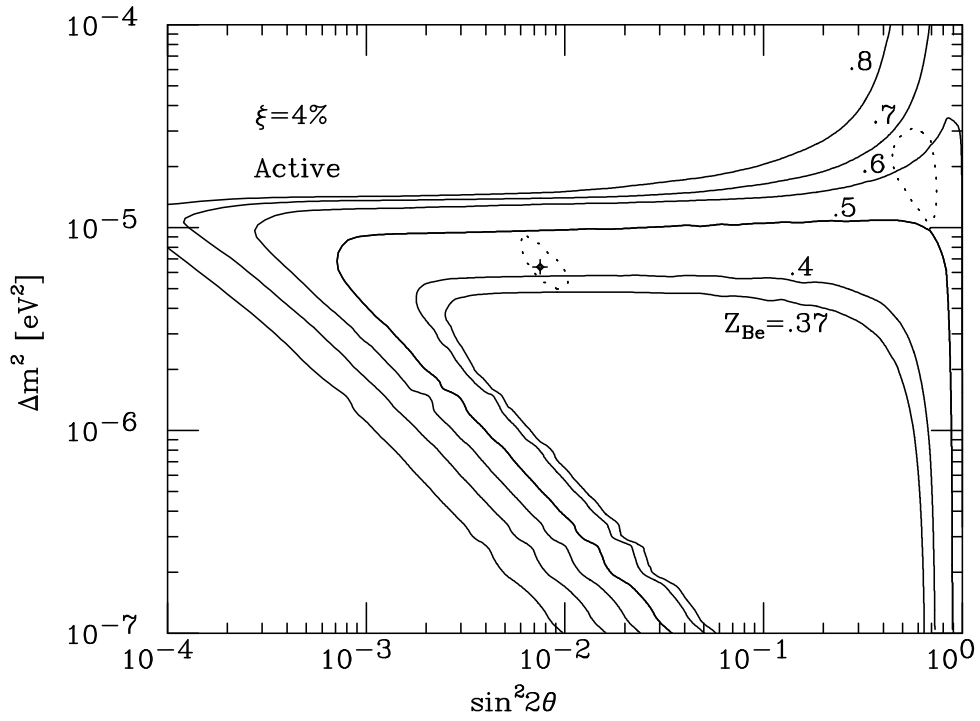


Fig. 4c

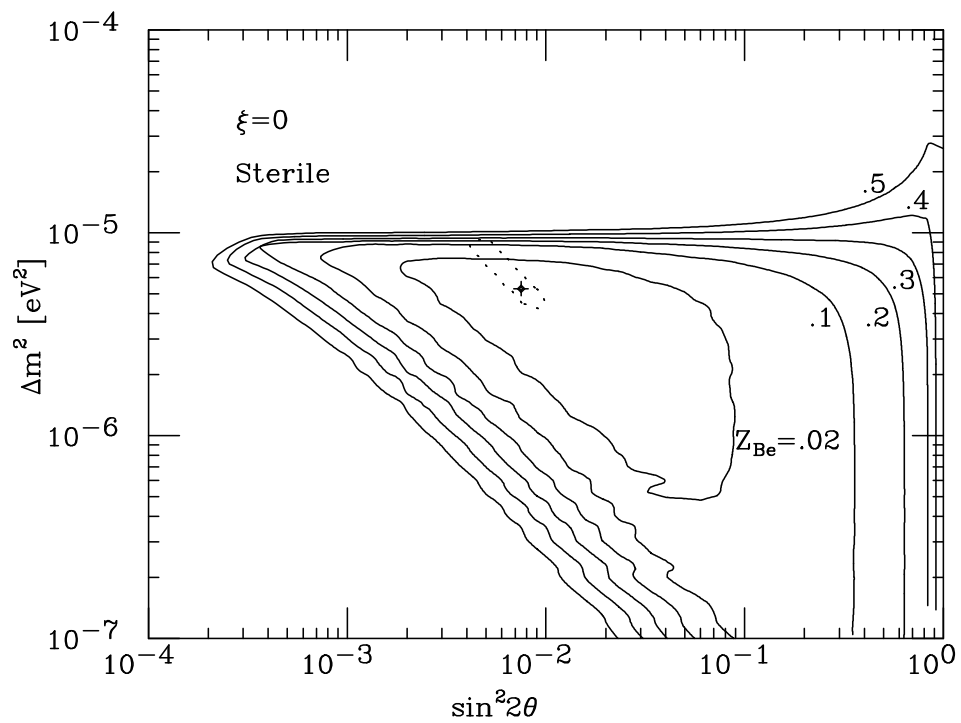


Fig. 4d

